

Write head design for effective curvature reduction in heat-assisted magnetic recording by topology optimization

O. Muthsam,^{1, a)} C. Vogler,¹ F. Bruckner,¹ and D. Suess¹

University of Vienna, Physics of Functional Materials, Boltzmannngasse 5, 1090 Vienna, Austria

(Dated: 18 October 2021)

The reduction of the transition curvature of written bits in heat-assisted magnetic recording (HAMR) is expected to play an important role for the future areal density increase of hard disk drives. Recently a write head design with flipped write and return poles was proposed. In this design a large spatial field gradient of the write head was the key to significantly reduce the transition curvature. In this work we optimized the write pole of a heat-assisted magnetic recording head in order to produce large field gradients as well as large fields in the region of the heat pulse. This is done by topology optimization. The simulations are performed with dolfin-adjoint. For the maximum field gradients of 8.1 mT/nm, 8.6 mT/nm and 11.8 mT/nm, locally resolved footprints of an FePt like hard magnetic recording medium are computed with a coarse-grained Landau-Lifshitz-Bloch (LLB) model and the resulting transition curvature is analysed. Additional simulations with a bilayer structure with 50% hard and 50% soft magnetic material are computed. The results show that for both recording media, the optimized head design does not lead to any significant improvement of the written track. Thus, we analyse the transition curvature for the optimized write heads theoretically with an effective recording time window (ERTW) model. Moreover, we check how higher field gradients influence the curvature reduction. The results show that a simple optimization of the conventional head design design is not sufficient for effective curvature reduction. Instead, new head concepts will be needed to reduce transition curvature.

I. INTRODUCTION

In heat-assisted magnetic recording (HAMR)^{1–4} a heat pulse is included to the writing process to overcome the so-called recording trilemma⁵ and make high-anisotropy grains writable with the available head fields. However, in granular media, the curved thermal profile of the heat pulse in combination with a spatially relatively homogeneous head field gives rise to a significant curvature at transitions between bits^{6,7}. This transition curvature is expected to be a serious problem for the read-back process in HAMR since the signal-to-noise ratio (SNR) is reduced⁸. Different methods to efficiently reduce transition curvature in HAMR have been proposed, for example a write head field design by Zhu *et al*^{8–10}. The present work is based on the publication by Vogler *et al*¹¹, where a recording head design with flipped write and return pole to efficiently reduce transition curvature is suggested. For the flipped head design writing of the bit happens between the near field transducer (NFT) and the returnpole, whereas for the conventional design writing happens near the write pole. The position where the bit is written for the different design is indicated by the grey arrows in Figure 1(a) and (b). The different writing position leads to a different behavior of the write field during the cooling process of the heat pulse. For the conventional design, the applied field is spatially relatively homogeneous during the cooling process (see Figure 1(c)). In contrast to this, shown in Figure 1(d), the field decreases during cooling for the flipped design which leads to a field gradient in down-track direction.

This field gradient turned out to be the key for the curvature reduction. For this reason, the head field gradient in down-track direction is an important parameter in the simulations.

In this work, we compute the realistic field gradient for a flipped design, that follows the model of a state-of-the-art recording head design^{12,13}, at the position where the heat pulse is cooling down. To optimize the head, we design a write pole that maximizes both the field and the field gradient at the required position. This is done by topology optimization¹⁴, an application of the inverse magnetostatic problem¹⁵. With the resulting fields and field gradients we compute locally resolved switching probability phase diagrams with a coarse-grained LLB model¹⁶ for both pure hard magnetic recording material and an exchange spring structure with 50% hard and 50% soft magnetic material. From this locally resolved phase diagrams, we can then analyse the transition curvature. Additionally, we interpret the results in the context of the effective recording time window (ERTW) model by Vogler *et al*^{11,36}. This paper is structured as follows: In Section II, a theoretical framework of the simulation methods is presented and the simulation and material parameters are given. The results are presented in Section III and discussed in Section IV.

II. THEORETICAL FRAMEWORK

A. Topology optimization

To solve the topology-optimization problem, the density method, which is also known as solid isotropic microstructure with penalization (SIMP), is used^{17,18}.

^{a)}Electronic mail: olivia.muthsam@univie.ac.at

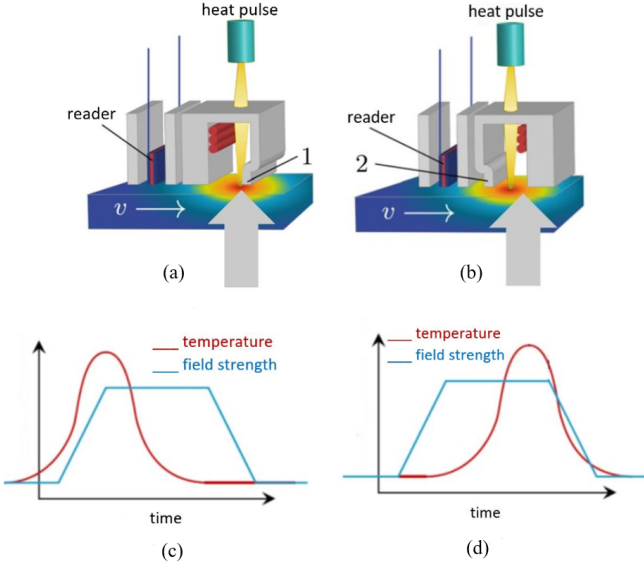


FIG. 1. Schematic representation of (a) a conventional and (b) a flipped recording head design proposed by Vogler *et al*¹¹. In (c) and (d) the temporal evolution of the applied field and the temperature pulse for the conventional and the flipped design, respectively, can be seen. The grey arrows in (a) and (b) indicate the position at which the grains are written.

First, the geometry is meshed with a tetrahedral mesh. At each element of the mesh the density ρ of the material is considered and a value between 0 (void) and 1 (material) is assigned to it. This leads to one optimization variable per element. The final design should only have density values of 0 or 1. This is achieved by using a penalization parameter k to penalize those densities that are intermediate.

The materials in the simulations are approximately described by linear material laws. For the soft magnetic material, the material law reads as

$$\mathbf{B}_s = \mu_0(\mathbf{H}_s + \mathbf{M}_s) = \mu_0\mu_r\mathbf{H}_s \quad (1)$$

where μ_r is the relative permeability. μ_0 denotes the vacuum permeability. For the hard magnetic material, there holds

$$\mathbf{B}_p = \mu_0\mu_m\mathbf{H}_p + \mu_0\mathbf{M}_0 \quad (2)$$

with the recoil permeability μ_m . For a permanent magnetic region $\Omega_p \subset \mathbb{R}^3$, the magnetization as a function of the density ρ can be written as

$$\mathbf{M}(\rho) = \rho^k\mathbf{M}_0 \quad (3)$$

with the density value $\rho \in [0, 1]$ of one element and the penalization parameter k . For hard magnetic materials, $k = 1$ is a good choice¹⁹. For a soft magnetic design region $\Omega_s \subset \mathbb{R}^3$, the magnetic susceptibility χ can be reformulated as a function of the density to

$$\chi(\rho) = \chi_0 \cdot \rho^k \quad (4)$$

and thus for the relative permeability, there holds

$$\mu_r(\rho) = (\mu_{r0} - 1)\rho^k + 1. \quad (5)$$

In this way it can be used for topology optimization. In the case of soft magnetic material, $k = 4$ leads to good results²⁰.

The topology-optimization problem that needs to be solved is given by

$$\begin{aligned} & \text{Find : } \min_{\rho} J(\rho) \\ & \text{subject to : } \int_{\Omega_i} \rho(r)dr \leq V; \\ & 0 \leq \rho(r) \leq 1, r \in \Omega_i \end{aligned} \quad (6)$$

where J is the objective function, V is the maximum volume of the design as a constraint and $i \in \{s, p\}$ defines the soft and permanent magnetic region, respectively. The objective function used to maximize the magnetic field and the z -field gradient is given by minimizing

$$\begin{aligned} J(\rho) = & \int_{\Omega_{\text{field}}} \frac{1}{|\nabla H_z(\rho)|^2} dr + \int_{\Omega_{\text{field}}} \frac{1}{|H_z(\rho)|^2} dr \\ & + \lambda \cdot \underbrace{\int_{\Omega_{\text{opt}}} \rho(1 - \rho) dr}_{\text{penalization}}, \end{aligned} \quad (7)$$

where Ω_{opt} is the region of the material that is optimized, $H_z(\rho)$ is the z -field and $\nabla H_z(\rho)$ is the gradient of the z -field. λ is a penalization parameter. The topology-optimization problem is solved by a finite element method (FEM) which is based on the open-source library FEniCS^{21,22} for solving partial differential equations (PDEs) and the library dolfin-adjoint^{23,24}. Dolfin-adjoint automatically determines and solves adjoint linear equations using PDEs which are discretized with finite elements. The minimization problem is solved using the L-BFGS-B method^{25,26}, a limited-memory quasi-Newton solver for bound-constrained optimization.

B. Head design parameters

In the topology-optimization simulations, a write head^{27,28} is optimized, which consists of a write and a return pole, a permanent magnet to simulate the core magnetized by a coil and a 50 nm thick soft magnetic underlayer (SUL). Additionally, in some simulations a backshield is considered. All components and the dimensions of the write head are marked in Figure 2 and summarized in Table I. The tip of the write pole and the backshield, if considered, are the parts of the write head that are optimized by topology optimization. Except the permanent magnet, all other parts of the write head consist of soft magnetic material.

The material of the recording head is assumed to be FeCo²⁹. Hence, a relative permeability $\mu_r = 18000$ and a saturation polarization of 2.4 T are assumed³⁰. It is

considered that the coil magnetizes the core with 0.8 T in x -direction which is modeled by the means of a permanent magnet that is magnetized in x -direction with 0.8 T. This field is chosen because then the maximum magnetization of the initial design is slightly below the saturation polarization of the material.

The field and the field gradient are computed and optimized at the position where the recording medium is hit by the heat spot produced by the NFT is already cooling down. This position is assumed to be 50 nm away from the pole tip in x -direction.

Since small head to media spacings (HMS) are needed, to get high areal storage density³¹, the HMS is assumed to be 5 nm.

Four different starting geometries are considered. The starting geometries are basic geometries of dimensions $x_{\text{write}} \times y_{\text{total}} \times z_{\text{opt}}$, where the density initially is 1 for each element. During the optimization process, the density of each element is adjusted. The difference between the geometries is the dimension in x -direction and the fact if a backshield is considered or not. The dimensions in y - and z -direction are the same for all starting geometries and equal to y_{total} and z_{opt} , respectively. The first geometry to be optimized, is one with dimension $x_{\text{write}} = 100$ nm and no backshield. This one is referred to as Basic₁₀₀. The second geometry also has dimension $x_{\text{write}} = 100$ nm. However, for this geometry a backshield with $x_{\text{back}} = 100$ nm is additionally considered and optimized. Afterwards, this geometry is called Backshield₁₀₀. The last geometries are similar to the former ones but with dimensions $x_{\text{write}} = 200$ nm and $x_{\text{back}} = 200$ nm. They are labeled Basic₂₀₀ and Backshield₂₀₀. The x_{write} and x_{back} values of the different geometries are summarized in Table II.

After the optimal head designs are determined via topology-optimization, additional simulations with magnum.fe³² that include a coil instead of a permanent magnet are performed. These coil-simulations are performed in order to determine realistic fields with the optimized head designs. Here, all parts of the write head are considered to be soft magnetic with the above material parameters. The current density inside the coil is assumed to be 2.5×10^{10} A/m², which is below the current density limit of 10^{12} A/m²,³³.

III. RESULTS

A. Field gradients

Forward simulations show that the field gradient of the initial flipped design, which follows a state-of-the-art head design^{12,13}, at 50 nm distance from the write pole is approximately 2.2 mT/nm. In Figure 3 the resulting fields from the coil simulations with the optimized geometries are plotted. The results show that the best outcome can be achieved for a geometry with a pole tip with $x_{\text{write}} = 200$ nm and an additional backshield with

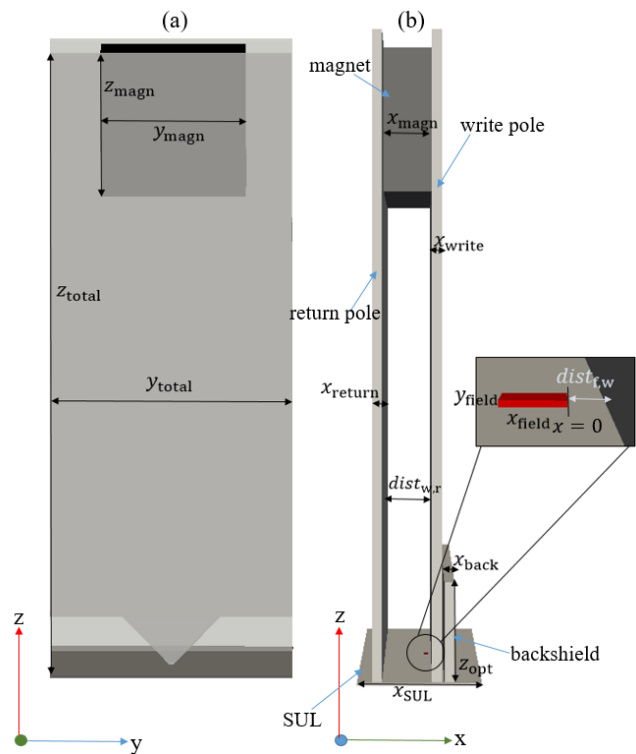


FIG. 2. Schematic representation with dimensions of the initial flipped head design. The dimensions can be seen in Table I. In (a) the front view and in (b) the side view can be seen. The 100 nm \times 100 nm wide fieldbox is 50 nm away from the write pole.

$x_{\text{back}} = 200$ nm. Here, the maximum field gradient is 11.8 mT/nm. The optimized Backshield₂₀₀ geometry is shown in Figure 4. Note that all optimized geometries are similar and show a tapered shape. Recapitulating, the resulting write fields and field gradients for the different geometries are summarized in Table II.

B. Curvature reduction

To analyse the curvature reduction, switching probability phase diagrams are computed with the help of a coarse-grained model based on the stochastic Landau-Lifshitz-Bloch equation (LLB)¹⁶ for a FePt like granular recording medium. The material parameters of the medium can be seen in Table III. In the simulations a continuous laser pulse with Gaussian shape and a full width at half maximum (FWHM) of 60 nm is considered. The temperature profile of the heat pulse is given by

$$T(x, y, t) = (T_{\text{write}} - T_{\text{min}})e^{-\frac{(x-vt)^2 + y^2}{2\sigma^2}} + T_{\text{min}} \quad (8)$$

$$= T_{\text{peak}}(y) \cdot e^{-\frac{(x-vt)^2}{2\sigma^2}} + T_{\text{min}} \quad (9)$$

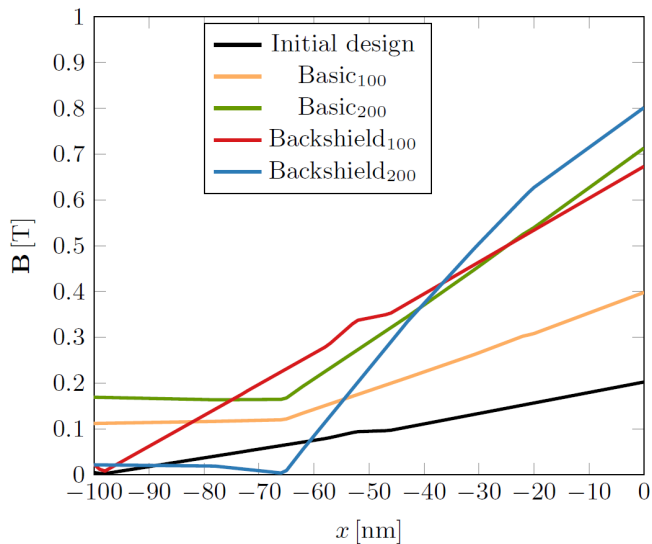
with

x_{SUL}	y_{total}	z_{total}	x_{magn}	y_{magn}	z_{magn}	z_{opt}	x_{write}	x_{return}	$\text{dist}_{\text{w,r}}$	x_{back}	$\text{dist}_{\text{f,w}}$	x_{field}	y_{field}
2 μm	5 μm	13 μm	1 μm	3 μm	3 μm	2 μm	varied	200 nm	1 μm	varied	50 nm	100 nm	100 nm

TABLE I. Approximated dimensions of an initial flipped recording head design as marked in Figure 2.

Geometrie	x_{write} [nm]	x_{back} [nm]	$\mu_0 H$ [T]	Max. $\mu_0 dH/dx$ [mT/nm]
Conventional	100	—	0.8	—
Initial flipped design	100	—	0.2	2.2
Basic ₁₀₀	100	—	0.4	4.1
Basic ₂₀₀	200	—	0.7	8.6
Backshield ₁₀₀	100	100	0.67	8.1
Backshield ₂₀₀	200	200	0.8	11.8

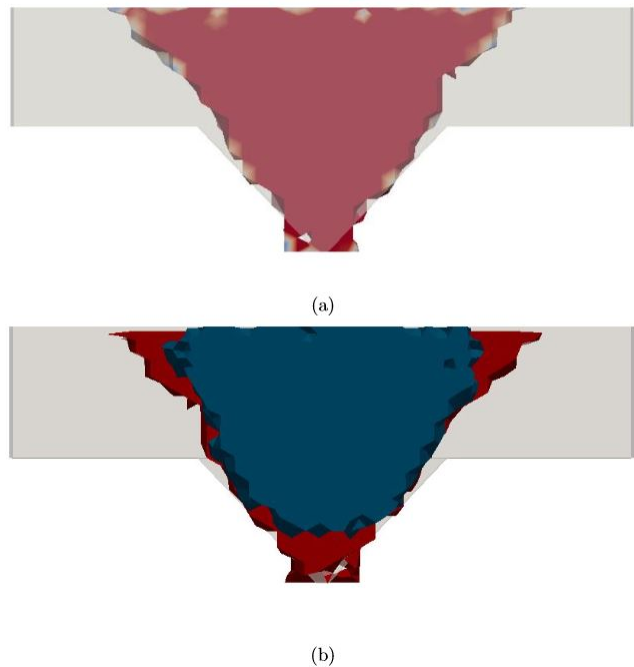
TABLE II. Resulting fields and field gradients produced by the write heads which are optimized with the help of topology optimization for a FeCo like head material. The field and its gradient of a conventional head are added for comparison.

FIG. 3. Comparison of the fields of the topology optimized geometries for a FeCo like head material. The magnetic field is plotted over the x -length of the 100 nm \times 100 nm wide fieldbox (marked red in Figure 2). At $x = 0$, the fieldbox is 50 nm away from the edge of the write pole.

$$\sigma = \frac{\text{FWHM}}{\sqrt{8 \ln(2)}}. \quad (10)$$

The speed v of the write head is assumed to be 15 m/s. x and y are the down-track and the off-track position of the grain, respectively. In the simulations both the down-track position x and the off-track position y are variable. The initial and final temperature of all simulations is $T_{\text{min}} = 300$ K. The write temperature T_{write} is chosen to be 800 K. The applied field is modeled as a trapezoidal field with a field duration of 0.57 ns and a field rise and fall time of 0.1 ns. The angle of the applied field with respect to the normal is assumed to be 22 deg. In each phase point 128 HAMR simulation simulations of a recording grain are performed.

In the phase diagrams the switching probability of a recording grain is shown as a function of the down-track position x and the off-track position y . First, the phase diagram is computed for a spatially homoge-

FIG. 4. Comparison of the initial flipped head design (grey) and the topology optimized write pole (red) with a backshield (blue) with $x_{\text{write}} = 200$ nm and $x_{\text{back}} = 200$ nm (red). (a) Front view and (b) rear view with backshield of the optimized write pole.

neous field which approximates a conventional recording head design. Additionally, footprints for optimized geometries with field gradients of 8.6 mT/nm (Basic₂₀₀), 8.1 mT/nm (Backshield₁₀₀) and 11.8 mT/nm (Backshield₂₀₀) are computed. The geometries with field gradients 2.2 mT/nm (Initial flipped) and 4.1 mT/nm (Basic₁₀₀) are not further considered since the phase diagrams show too much noise to get reliable results. Note, that different write fields (see Table II) are used for the simulations with different field gradients as seen in Table II. In Figure 5, the resulting switching probability phase diagrams can be seen. There are some visible differences between the footprints of the different field gradients.

One can see that for the flipped designs the recording performance is worse than for the conventional design

where a homogeneous field is assumed. This can be seen by the increase of jitter in down-track direction and the reduction of the maximum switching probability P_{\max} . P_{\max} and the jitter can be determined by fitting the $P(x)$ -curve at one temperature with a Gaussian cumulative distribution function

$$\Phi_{\mu,\sigma^2} = \frac{1}{2} \left(1 + \operatorname{erf} \left(\frac{x - \mu}{\sqrt{2\sigma^2}} \right) \right) \cdot p \quad (11)$$

with

$$\operatorname{erf}(x) = \frac{2}{\sqrt{\pi}} \int_0^x e^{-\tau^2} d\tau, \quad (12)$$

where the fitting parameters are the mean value μ , the standard deviation σ and the mean maximum switching probability $p \in [0, 1]$. The standard deviation σ determines the steepness of the transition function and is a measure for the transition jitter. The temperature at which the down-track jitter is determined is $T_{\text{peak}} = 760$ K. The resulting jitter and P_{\max} values are summarized in Table IV. Additionally, it can be seen that the grains are written at larger off-track positions for increasing field gradients and the resulting lower write fields. The various write fields lead to writing of the grains at different peak temperatures. For smaller write fields the grains are written at higher temperatures only whereas they are written at lower temperatures for higher fields. The convention

$$T_{\text{peak}}(y) = (T_{\text{write}} - T_{\text{min}}) e^{-\frac{y^2}{2\sigma^2}} + T_{\text{min}}. \quad (13)$$

shows that with higher write fields, the off-track edge of a bit shifts to larger off-track positions, because the minimum temperature necessary to write a grain is smaller.

For a detailed analysis of the transition curvature, the full down-track range Δx in which the bit is written with $P_{\max} \geq 50\%$ is computed. Δx is marked in Figure 5 as the distance between the black dashed lines. Because of the different off-track widths Δy in the phase diagrams for the different geometries, it is necessary to scale the curvature parameter with Δy . This is done, since the track width is usually kept constant in magnetic recording. In reality the track-width can for example be steered by controlling the peak temperature T_{peak} or the full width at half maximum³⁴. With the curvature parameter $c = \Delta x / \Delta y$, the curvature can be reliably analyzed. Note that c is equivalent to the curvature parameter used by Vogler *et al*¹¹ when multiplied by Δy for scaling reasons. There holds

$$c = \frac{\Delta x}{\Delta y} \equiv cp \cdot \Delta y \quad (14)$$

where cp is the curvature parameter defined by Vogler *et al*¹¹. The curvature analysis shows that the curvature

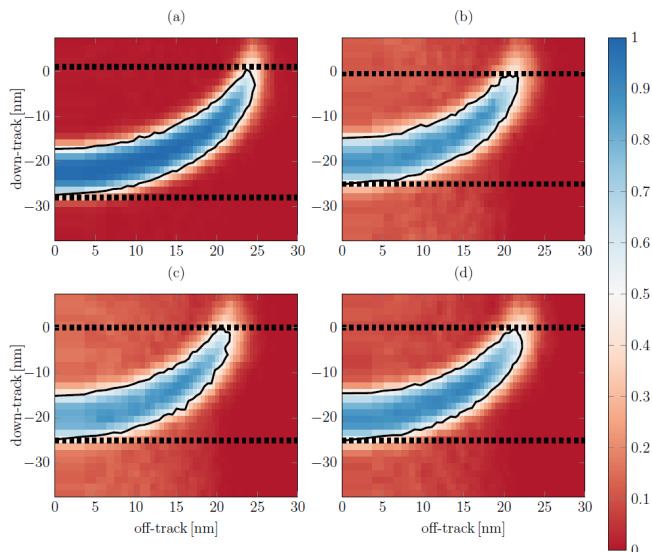


FIG. 5. Switching probability phase diagrams of (a) a conventional head with a homogeneous write field and the flipped design with optimized field gradients (b) $\mu_0 dH/dx = 8.6$ mT/nm (Basic₂₀₀), (c) $\mu_0 dH/dx = 8.1$ mT/nm (Backshield₁₀₀) and (d) $\mu_0 dH/dx = 11.8$ mT/nm (Backshield₂₀₀) in combination with pure hard magnetic recording material. The black dashed lines indicate the maximum and minimum down-track position x with $P(x) = 50\%$.

is increased for both the Basic₂₀₀ and the Backshield₁₀₀ design compared to the conventional design. The curvature reduction for the Backshield₂₀₀ flipped head design with a field gradient of 11.8 mT/nm is about 1.3%. Detailed information about the curvature parameters can be seen in Table IV.

C. Exchange Spring Recording Medium

Since the curvature reduction is negligible for pure hard magnetic recording media in combination with the flipped head design, a bilayer structure with 50% hard and 50% soft magnetic material is tested as recording material. In the original paper by Vogler *et al*¹¹, a bilayer structure showed significantly higher curvature reduction than the pure hard magnetic recording medium. The total height of the grains is again $h = 8$ nm. The material parameters of the soft magnetic composition can be seen in Table V. Phase diagrams for the different head designs are calculated and the off-track width is again normalized for comparability reasons. They are shown in Figure 6. Again, the jitter σ_{down} and P_{\max} are calculated for the footprints and compared in Table VI. Due to the higher Curie temperature of the exchange spring recording medium, the down-track jitter is determined at 800 K. For the exchange spring recording material the behavior of the curvature is similar to that for pure hard magnetic recording media and seems to be even worse. For the Backshield₂₀₀ head design the decrease of the curvature is only 0.08% compared to the conventional de-

Curie temp. T_C (K)	Damping α	Anisotropy const. K_1 (MJ/m ³)	Anisotropy field $\mu_0 H_k$ (T) at 300 K	J_s (T)	height h (nm)	diameter d (nm)
693.5	0.02	6.6	10	1.35	8	5

TABLE III. Material parameters of a FePt like hard magnetic granular recording medium. Note, that different material parameters for the recording medium were used compared to the original work of Vogler *et al*¹¹.

Geometry	c (%)	P_{\max} (%)	σ_{down} (%)
Basic ₂₀₀	+1.4	-5.5	+118.7
Backshield ₁₀₀	+3.8	-7	+113.5
Backshield ₂₀₀	-1.35	-2.3	+28.4

TABLE IV. Resulting transition curvature, P_{\max} and jitter parameters of the different flipped head designs in combination with a pure hard magnetic recording material compared to a conventional recording head design.

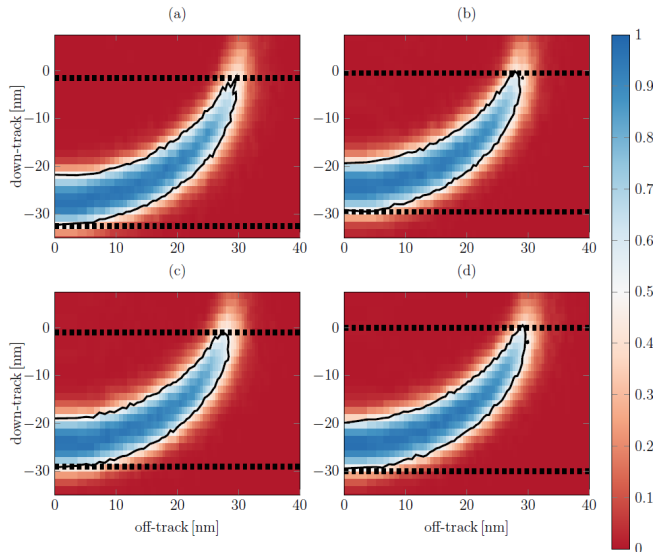


FIG. 6. Switching probability phase diagrams of (a) a conventional head with a homogeneous write field and the flipped design with optimized field gradients (b) $\mu_0 dH/dx = 8.6$ mT/nm (Basic₂₀₀), (c) $\mu_0 dH/dx = 8.1$ mT/nm (Backshield₁₀₀) and (d) $\mu_0 dH/dx = 11.8$ mT/nm (Backshield₂₀₀) in combination with an exchange spring bilayer structure. The black dashed lines indicate the maximum and minimum down-track position x with $P(x) = 50\%$.

sign. However, the maximum switching probability stays 100% and the down-track jitter decreases.

D. Comparison with ERTW model

To understand why both the pure hard magnetic and the exchange spring media show almost no curvature reduction, the results are compared to theoretical considerations with the effective recording time window (ERTW) model described by Vogler *et al*^{11,36}. The effective recording time window (ERTW) is defined by^{35,36}

$$\text{ERTW}_{\uparrow} = [t(T_c), t(T_{\text{freeze}})] \cap [t_{\uparrow, \text{start}}, t_{\uparrow, \text{final}}] \quad (15)$$

The first term on the right hand side gives the time window in which the grains can be written in HAMR, namely in the temperature range between the Curie temperature T_c and the freezing temperature T_{freeze} . At the freezing temperature the coercivity decreases below the given field strength such that the grain cannot be written any longer. To calculate the ERTW, the freezing temperature has to be estimated. For this reason, hysteresis loops are simulated for various temperatures with VAMPIRE⁵. At each fixed temperature, 128 hysteresis loops are computed and the temperature dependence of the coercive field dH_c/dT is determined. If the coercive field at a fixed temperature is lower than the write field, the temperature is a possible write temperature. Since the magnitude of the write field is not constant for the flipped head designs, a correction factor is included in the model. With the correction factor the magnitude of the field is updated according to the field gradient and the resulting write field is used for the determination of the freezing temperature.

The second term gives the time window in which the field points in the desired write direction, which in the following is regarded as pointing upwards without loss of generality. With this ERTW definition a switching probability phase diagram without noise can be computed for different materials and various fields and field gradients. The switching probability of a recording grain can be computed via³⁶

$$p = \min\left(\frac{\text{ERTW}_{\uparrow}}{\Theta_{\text{ERTW}}}, 1\right) \left[1 - \min\left(\frac{\text{ERTW}_{\downarrow}}{\Theta_{\text{ERTW}}}, 1\right)\right]. \quad (16)$$

The first term gives the probability that a bit is written in write direction. Since the probability cannot exceed 1, the minimum between 1 and Θ_{ERTW} is taken. Θ_{ERTW} is a threshold of the ERTW that gives the time that must be exceeded for successful switching to occur. It can be determined as a fit parameter to reproduce the results by the LLB model. The second term is the probability that a grain is overwritten after it was already aligned in write direction. Together, p describes the joint probability to switch a bit in write direction and not reverting it afterwards. From the phase diagrams, the transition curvature is calculated and it is determined how much the theoretical curvature reduction should be.

For the Backshield₂₀₀ geometry, the theoretically expected curvature reduction is about 1% for the pure

Curie temp. T_C (K)	Damping α	Anisotropy const. K_1 (MJ/m ³)	J_s (T)
740.9	0.1	0	1.35

TABLE V. Material parameters of the soft magnetic composition of the bilayer structure.

Geometry	c (%)	P_{\max} (%)	σ_{down} (%)
Basic ₂₀₀	+1.38	-2.5	-16.2
Backshield ₁₀₀	+1.9	-1.19	-4.7
Backshield ₂₀₀	-0.08	+/- 0.0	-19

TABLE VI. Resulting transition curvature, P_{\max} and jitter parameters of the different flipped head designs in combination with an exchange spring recording medium compared to a conventional recording head design with the same recording material.

hard magnetic recording material compared to the conventional design. This agrees very good with the curvature reduction resulting from the LLB simulations. For the exchange spring bilayer structure, the ERTW model predicts a curvature reduction of about 1.7%. The very small value achieved by the LLB simulation (-0.08%) results from the switch of the transition around zero. This switch does not happen in the analytical ERTW model and comes from the stochastic nature of the LLB model. Additionally, with the ERTW model, it can be analyzed with reasonable computational effort how the transition curvature reduction depends on the field gradient. The resulting curvature reduction values can be seen in Table VII. They display that the curvature reduces linearly with the field gradient. Moreover, a higher potential for the curvature reduction can be seen for the exchange spring bilayer structure. However, even with field gradients up to 40 mT/nm, the bilayer structure did not show as high curvature reduction as the exchange spring media used by Vogler *et al.* This can most likely be explained by the different damping constants used in the hard magnetic material. In the work by Vogler *et al.*, the damping constant is $\alpha_{\text{HM}} = 0.1$ whereas it is $\alpha_{\text{HM}} = 0.02$ in this work. This leads to different dH_c/dT gradients and thus to the different curvature behavior. This shows that damping plays a key role for the curvature reduction.

IV. DISCUSSION

To conclude, in this work we tried to optimize the design of the write pole of a recording head for heat-assisted magnetic recording in order to reduce transition curvature. The write pole of the head was optimized in a way to maximize both the z -field and the z -field gradient at the position where the applied heat pulse is cooling down. This was done with the help of topology optimization which is an application of the inverse magnetostatic problem. Different starting geometries were considered. The comparison of the different geometries to a conventional recording head design showed the best results for a write pole and an additional backshield which both have dimension 200 nm in down-track direction. The resulting field gradient is then 11.8 mT/nm. The optimized geometries are all similar. They all have smooth edges, a tapered shape with a tip in the middle and the peak is

skewed in x -direction such that the distance of the pole tip to the recording medium is close to the fieldbox and larger on the side away from it (see Figure 4). Since all optimized geometries are similar, the field and the field gradient could be maximized further by optimizing even larger write poles with an additional backshield. Another option to further increase the field gradient produced by the write pole is a design where the NFT is closer to the write pole.

We calculated switching probability phase diagrams of FePt like head magnetic recording media for the different optimized field gradients. It is noteworthy that the switching performance, in terms of down-track jitter and maximum switching probability, for all flipped head designs is worse than that of the conventional head design. Both, the AC and the DC noise increase for the flipped head designs. The performance loss results most likely from the smaller write fields that are produced by the flipped head designs. Analyzing the transition curvature showed that the curvature reduces only marginally even for the Backshield₂₀₀ design where the highest write field and field gradient can be achieved. An idea how to improve the curvature reduction is to use an exchange spring medium³⁷⁻⁴². The soft magnetic layer acts as a write assist and thus smaller write fields are required to write the grains. For the conventional design the curvature of the exchange spring recording medium is larger than that of the pure hard magnetic medium. Thus, the curvature reduction potential was expected to be higher for the exchange spring media. We computed switching probability phase diagrams for the different head designs in combination with the exchange spring recording media. Surprisingly, the curvature reduction for the Backshield₂₀₀ design was even smaller than for the pure hard magnetic material. To understand why the curvature reduces only so little, we analyzed the results in the context of the effective recording time window (ERTW) model that was used in the paper by Vogler *et al.*¹¹. The ERTW model confirmed the results of the LLB model. Hence, we can conclude that the marginal reduction of the curvature is not a consequence of noise. The analysis also pointed out that the exchange spring recording medium shows a larger potential for curvature reduction if higher field gradients are used but even here the curvature reduction is only marginally.

In conclusion, we did not see any improvement of the transition curvature for the resulting field gradients of

Field gradient [mT/nm]	c (%) HM	c (%) HM/SM
12	-1.0	-1.7
16	-1.6	-3.64
20	-2.09	-5.58
24	-2.59	-7.5
28	-3.38	-9.48
32	-4.6	-11.4
36	-5.2	-13.11
40	-5.8	-14.2

TABLE VII. Curvature reduction in % compared to a conventional design for pure hard magnetic recording material (HM) and an exchange spring bilayer structure (HM/SM) calculated with the ERTW model.

the optimized flipped head design in combination with pure hard magnetic and exchange spring recording media. The results showed that a simple optimization of the conventional head design is not sufficient for effective curvature reduction but that new head concepts have to be introduced to reduce transition curvature.

V. ACKNOWLEDGEMENTS

The authors would like to thank the Vienna Science and Technology Fund (WWTF) under grant No. MA14-044, the Advanced Storage Technology Consortium (ASTC), and the Austrian Science Fund (FWF) under grant No. I2214-N20 for financial support. The computational results presented have been achieved using the Vienna Scientific Cluster (VSC).

- ¹Hiroshi Kobayashi, Motoharu Tanaka, Hajime Machida, Takashi Yano, and Uee Myong Hwang. *Thermomagnetic recording*. Google Patents, August 1984.
- ²C. Mee and G. Fan. A proposed beam-addressable memory. *IEEE Transactions on Magnetism*, 3(1):72–76, 1967.
- ³Robert E. Rottmayer, Sharat Batra, Dorothea Buechel, William A. Challener, Julius Hohlfeld, Yukiko Kubota, Lei Li, Bin Lu, Christophe Mihalcea, Keith Mountfield, and others. Heat-assisted magnetic recording. *IEEE Transactions on Magnetism*, 42(10):2417–2421, 2006.
- ⁴Mark H. Kryder, Edward C. Gage, Terry W. McDaniel, William A. Challener, Robert E. Rottmayer, Ganping Ju, Yiao-Tee Hsia, and M. Fatih Erden. Heat assisted magnetic recording. *Proceedings of the IEEE*, 96(11):1810–1835, 2008.
- ⁵R. F. L. Evans, Roy W. Chantrell, Ulrich Nowak, Andreas Lyberatos, and H.-J. Richter. Thermally induced error: Density limit for magnetic data storage. *Applied Physics Letters*, 100(10):102402, 2012.
- ⁶Nan Zhou, Xianfan Xu, Aaron T. Hammack, Barry C. Stipe, Kaizhong Gao, Werner Scholz, and Edward C. Gage. Plasmonic near-field transducer for heat-assisted magnetic recording. *Nanophotonics*, 3(3), January 2014.
- ⁷Jacek Gosciniaik, Marcus Mooney, Mark Gubbins, and Brian Corbett. Novel droplet near-field transducer for heat-assisted magnetic recording. *Nanophotonics*, 4(1), January 2015.
- ⁸J. G. J. Zhu and H. Li. Correcting Transition Curvature in Heat-Assisted Magnetic Recording. *IEEE Transactions on Magnetism*, 53(2):1–7, February 2017.
- ⁹Jian-Gang (Jimmy) Zhu and Hai Li. Write head field design for correcting transition curvature in heat assisted magnetic recording. *AIP Advances*, 7(5):056505, February 2017.
- ¹⁰Yuwei Qin, Hai Li, and Jian-Gang Zhu. Curvature-Eliminating Head Field and Track Edge Characteristics in Heat-Assisted Magnetic Recording. *IEEE Transactions on Magnetism*, 53(11):1–4, 2017.
- ¹¹Christoph Vogler, Claas Abert, Florian Bruckner, and Dieter Suess. Efficiently reducing transition curvature in heat-assisted magnetic recording with state-of-the-art write heads. *Applied Physics Letters*, 110(18):182406, May 2017.
- ¹²Sung-dong Suh, Young-hun Im, and Hae-Sung Kim. Heat-assisted magnetic recording head, October 2009.
- ¹³Myung-bok Lee and Jin-Seung Sohn. Heat assisted magnetic recording head, July 2007.
- ¹⁴Martin Philip Bendsøe and Ole Sigmund. *Topology Optimization: Theory, Methods, and Applications*. Springer Science & Business Media, April 2013. Google-Books-ID: ZCjsCAAQBAJ.
- ¹⁵Florian Bruckner, Claas Abert, Gregor Wautischer, Christian Huber, Christoph Vogler, Michael Hinze, and Dieter Suess. Solving Large-Scale Inverse Magnetostatic Problems using the Adjoint Method. *Scientific Reports*, 7:40816, January 2017.
- ¹⁶Christoph Vogler, Claas Abert, Florian Bruckner, and Dieter Suess. Landau-Lifshitz-Bloch equation for exchange-coupled grains. *Physical Review B*, 90(21):214431, 2014.
- ¹⁷C. Huber, C. Abert, F. Bruckner, C. Pfaff, J. Kriwet, M. Groenefeld, I. Teliban, C. Vogler, and D. Suess. Topology optimized and 3d printed polymer-bonded permanent magnets for a predefined external field. *Journal of Applied Physics*, 122(5):053904, August 2017.
- ¹⁸Claas Abert, Christian Huber, Florian Bruckner, Christoph Vogler, Gregor Wautischer, and Dieter Suess. A fast finite-difference algorithm for topology optimization of permanent magnets. *Journal of Applied Physics*, 122(11):113904, 2017.
- ¹⁹Jae Seok Choi and Jeonghoon Yoo. Simultaneous structural topology optimization of electromagnetic sources and ferromagnetic materials. *Computer Methods in Applied Mechanics and Engineering*, 198(27-29):2111–2121, May 2009.
- ²⁰Christian Huber. *3D printed polymer-bonded NdFeB magnets for a tailored magnetic field*. PhD thesis, TU Wien, 2017.
- ²¹Todd Dupont, Johan Hoffman, Claus Johnson, Robert C. Kirby, Mats G. Larson, Anders Logg, and L. Ridgway Scott. *The fenics project*. Chalmers Finite Element Centre, Chalmers University of Technology, 2003.
- ²²Martin S. Alna es, Jan Blechta, Johan Hake, August Johansson, Benjamin Kehlet, Anders Logg, Chris Richardson, Johannes Ring, Marie E. Rognes, and Garth N. Wells. The FEniCS project version 1.5. *Archive of Numerical Software*, 3(100):9–23, 2015.
- ²³S W Funke and P E Farrell. A framework for automated PDE-constrained optimisation. *ACM Transactions on Mathematical Software*, page 28.
- ²⁴P. E. Farrell, D. A. Ham, S. W. Funke, and M. E. Rognes. Automated Derivation of the Adjoint of High-Level Transient Finite Element Programs. *SIAM Journal on Scientific Computing*, 35(4):C369–C393, January 2013.
- ²⁵Richard H. Byrd, Peihuang Lu, Jorge Nocedal, and Ciyou Zhu. A limited memory algorithm for bound constrained optimization. *SIAM Journal on Scientific Computing*, 16(5):1190–1208, 1995.
- ²⁶Ciyou Zhu, Richard H. Byrd, Peihuang Lu, and Jorge Nocedal. Algorithm 778: L-BFGS-B: Fortran subroutines for large-scale bound-constrained optimization. *ACM Transactions on Mathematical Software (TOMS)*, 23(4):550–560, 1997.
- ²⁷Michael Allen Seigler, Mark William Covington, Michael Leigh Mallary, Hua Zhou, and Amit Vasant Itagi. Recording head for heat assisted magnetic recording, May 2013.

- ²⁸James A. Brug, Thomas C. Anthony, and Janice H. Nickel. Magnetic Recording Head Materials. *MRS Bulletin*, 21(09):23–27, September 1996.
- ²⁹M.T. Kief and R.H. Victora. Materials for heat-assisted magnetic recording. *MRS Bulletin*, 43(02):87–92, February 2018.
- ³⁰Y. Okada, H. Hoshiya, T. Okada, and M. Fuyama. Magnetic properties of FeCo multilayered films for single pole heads. *IEEE Transactions on Magnetics*, 40(4):2368–2370, July 2004.
- ³¹J. D. Kiely, P. M. Jones, H. Wang, R. Yang, W. Scholz, M. Benakli, J. L. Brand, and S. Gangopadhyay. Media Roughness and Head-Media Spacing in Heat-Assisted Magnetic Recording. *IEEE Transactions on Magnetics*, 50(3):132–136, March 2014.
- ³²Claas Abert, Lukas Exl, Florian Bruckner, Andr Drews, and Dieter Suess. magnum.fe: A micromagnetic finite-element simulation code based on FEniCS. *Journal of Magnetism and Magnetic Materials*, 345:29–35, November 2013.
- ³³Hendrik F Hamann, Prakash Kasiraj, Jeffrey S Lille, Yves C Martin, Chie Ching Poon, Neil Leslie Robertson, Jan-Ulrich Thiele, and Hemantha Kumar Wickramasinghe. Heating device and magnetic recording head for thermally-assisted recording, August 28 2007. US Patent 7,262,936.
- ³⁴Pin-Wei Huang and Randall H Victora. Heat assisted magnetic recording: Grain size dependency, enhanced damping, and a simulation/experiment comparison. *Journal of Applied Physics*, 115(17):17B710, 2014.
- ³⁵Jian-Gang Zhu and Hai Li. Understanding signal and noise in heat assisted magnetic recording. *IEEE Transactions on Magnetics*, 49(2):765–772, 2013.
- ³⁶Christoph Vogler, Claas Abert, Florian Bruckner, Dieter Suess, and Dirk Praetorius. Basic noise mechanisms of heat-assisted-magnetic recording. *Journal of Applied Physics*, 120(15):153901, 2016.
- ³⁷Dieter Suess, Thomas Schrefl, S. Fhler, Markus Kirschner, Gino Hrkac, Florian Dorfbauer, and Josef Fidler. Exchange spring media for perpendicular recording. *Applied Physics Letters*, 87(1):012504, 2005.
- ³⁸Jian-Ping Wang, Weikang Shen, and Jianmin Bai. Exchange coupled composite media for perpendicular magnetic recording. *IEEE transactions on magnetics*, 41(10):3181–3186, 2005.
- ³⁹R. H. Victora and X. Shen. Exchange coupled composite media for perpendicular magnetic recording. *IEEE Transactions on Magnetics*, 41(10):2828–2833, October 2005.
- ⁴⁰Dieter Suess. Micromagnetics of exchange spring media: Optimization and limits. *Journal of magnetism and magnetic materials*, 308(2):183–197, 2007.
- ⁴¹Kevin Robert Coffey, Jan-Ulrich Thiele, and Dieter Klaus Weller. *Thermal springmagnetic recording media for writing using magnetic and thermal gradients*. Google Patents, April 2005.
- ⁴²Dieter Suess and Thomas Schrefl. Breaking the thermally induced write error in heat assisted recording by using low and high Tc materials. *Applied Physics Letters*, 102(16):162405, 2013.
- ⁴³W. A. Challener, Chubing Peng, A. V. Itagi, D. Karns, Wei Peng, Yingguo Peng, XiaoMin Yang, Xiaobin Zhu, N. J. Gokemeijer, Y.-T. Hsia, G. Ju, Robert E. Rottmayer, Michael A. Seigler, and E. C. Gage. Heat-assisted magnetic recording by a near-field transducer with efficient optical energy transfer. *Nature Photonics*, 3(4):220–224, April 2009.
- ⁴⁴M. Hashimoto, M. Salo, Y. Ikeda, A. Moser, R. Wood, and H. Muraoka. Analysis of written transition curvature in perpendicular magnetic recording from spin-stand testing. *IEEE transactions on magnetics*, 43(7):3315–3319, 2007.